Production of 8.4 m segments for the Giant Magellan Telescope

H. M. Martin[a], R. G. Allen[a], J. H. Burge[a,b], D. W. Kim[b], J. S. Kingsley[a], K. Law[a], R. D. Lutz[a], P. A. Strittmatter[a], P. Su[b], M. T. Tuell[a], S. C. West[a] and P. Zhou[b]

[a]Steward Observatory, University of Arizona, Tucson, AZ 85721, USA
[b]College of Optical Sciences, University of Arizona, Tucson, AZ 85721, USA

ABSTRACT

Production of segments for the Giant Magellan Telescope is well underway at the Steward Observatory Mirror Lab. We report on the completion of the first 8.4 m off-axis segment, the casting of the second segment, and preparations for manufacture of the remaining segments. The complete set of infrastructure for serial production is in place, including the casting furnace, two 8.4 m capacity grinding and polishing machines, and a 28 m test tower that incorporates four independent measurement systems. The first segment, with 14 mm p-v aspheric departure, is by some measures the most challenging astronomical mirror ever made. Its manufacture took longer than expected, but the result is an excellent figure and demonstration of valuable new systems that will support both fabrication and measurement of the remaining segments. Polishing was done with a 1.2 m stressed lap for smoothing and large-scale figuring, and a series of smaller passive rigid-conformal laps for deterministic figuring on smaller scales. The interferometric measurement produces a null wavefront with a 3-element asymmetric null corrector including a 3.8 m spherical mirror and a computer-generated hologram. In addition to this test, we relied heavily on the new SCOTS slope test with its high accuracy and dynamic range. Evaluation of the measured figure includes simulated active correction using both the 160-actuator mirror support and the alignment degrees of freedom for the off-axis segment.

Keywords: Giant Magellan Telescope, telescopes, optical fabrication, optical testing, off-axis, aspheres, active optics

1. INTRODUCTION

Among the extremely large telescopes of the next generation, the Giant Magellan Telescope (GMT) is unique in using segments comparable to the size of the largest existing telescopes.[1],[2] Each of the seven segments is a lightweight honeycomb mirror similar to the primary mirrors for the 6.5 m MMT and Magellan telescopes and the 2x8.4 m Large Binocular Telescope. This choice of segment guarantees a smooth wavefront over 8.4 m subapertures and greatly reduces the number of elements that must be controlled to high accuracy in the telescope. With each primary mirror segment matched to a segment in the 3.25 m secondary mirror, the critical alignment and phasing of the pupil will be done with the seven small, agile secondary segments which are also the deformable mirrors for adaptive optics.

This minimally segmented design transfers much of the challenge of wavefront control from telescope operation to manufacture of the mirrors. Each primary mirror segment is 10 times more aspheric than the most aspheric large telescope mirrors to date (the LBT primaries, with 1.4 mm p-v aspheric departure). Polishing such an aspheric surface is challenging, and measuring it requires a set of tests unlike anything ever built before. Manufacture of the first segment has been seen as the most important technical demonstration for the GMT, and this demonstration has now been achieved.

In the process, the Steward Observatory Mirror Lab has developed all the infrastructure needed for serial production of the remaining segments. In addition to the casting furnace, the lab has two 8.4 m machines for grinding and polishing the segments; a 28 m test tower supporting four separate optical tests with optics up to 3.8 m diameter and precise mechanics up to 9 m dimensions; and tools and techniques for efficient figuring of mirrors. The second segment has already been cast, and the mold is being prepared for the casting of the third segment in August 2013. The Mirror Lab will continue to refine the equipment and techniques to improve the accuracy and efficiency for future segments, but the necessary pieces have been built and demonstrated.

Sections 2-4 of this paper summarize the fabrication and testing of the first segment and present the quality of the finished mirror. Section 5 describes the spin-casting of the second off-axis segment, and Section 6 describes the status and plans for the remaining segments.

Modern Technologies in Space- and Ground-based Telescopes and Instrumentation II,
edited by Ramón Navarro, Colin R. Cunningham, Eric Prieto, Proc. of SPIE Vol. 8450, 84502D
 · doi: 10.1117/12.926347

2. FABRICATION OF SEGMENT 1

The design and early stages of fabrication for the GMT segments have been described in previous papers.[3]-[5] We will describe the spin-casting process in Section 5. Here we discuss the figuring of the optical surface. The spin-casting produces a symmetric parabolic surface, so the off-axis surface with its 14 mm of aspheric departure was created during the initial machining. Loose-abrasive grinding and initial polishing were done with a 1.2 m stressed lap that had previously been used for the MMT, Magellan and LBT mirrors. The stressed lap changes its shape under computer control so it always matches the local curvature of the mirror. These shape changes for the off-axis segment require different software but the same hardware used for the axisymmetric mirrors. Although the GMT segment is ten times more aspheric than an LBT mirror, the fact that the aspheric departure is primarily astigmatism rather than spherical aberration means the magnitude of shape change over the 1.2 m lap is similar for the two mirrors. Figure 1 shows the stressed lap polishing the GMT surface.

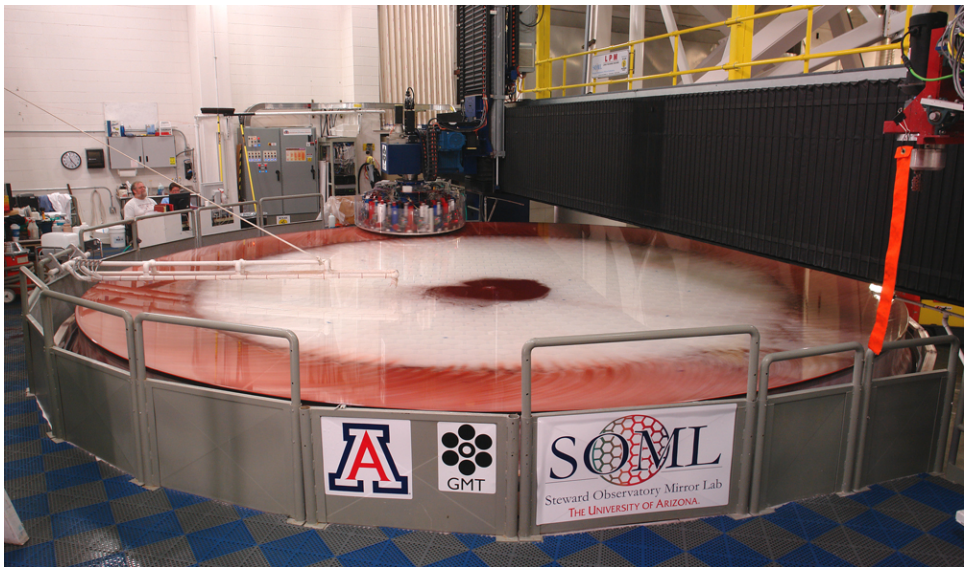

Figure 1. A 1.2 m stressed lap on one spindle of the polishing machine, being used to polish the GMT segment. Photo by Ray Bertram, Steward Observatory.

We expected that the stressed lap would accommodate the asymmetric surface and allow the opticians to figure the mirror as if it were symmetric. We can address large-scale non-axisymmetric figure errors by dynamically varying the polishing pressure and pressure gradients across the lap. On previous mirrors we have also used tools of 10-30 cm diameter for local figuring, especially near the edge. For symmetric mirrors these small-scale errors are generally axisymmetric and can be corrected with a simple system. We have been able to achieve accurate figures of about 20 nm rms surface error with this combination of tools and techniques.

We found, however, that the stressed lap was not as effective at controlling the figure of the GMT mirror as it had been for the axisymmetric mirrors. This was not expected and led to some delays. We don't fully understand the reason for the limitation and continue to investigate it. The general symptom is that axisymmetric polishing strokes (where dwell, relative speed and pressure depend only on distance from the center of the segment) produced non-axisymmetric figure changes. Some of these figure changes were on such small scales—a fraction of the lap diameter—that we could not correct them by varying the polishing pressure and pressure gradients as a function of position.

At the time we were experiencing difficulty with the stressed lap system, Kim and Burge were developing a small-tool polishing capability for other projects at the University of Arizona College of Optical Sciences.[6],[7] Their system provides full 2-dimensional figuring by varying the dwell of an orbital or rotating lap as it moves in a raster or spiral pattern. It is often used with a rigid-conformal (RC) lap that includes a visco-elastic layer that is stiff on short time scales and soft on longer timescales, so it can flow to accommodate aspheric surfaces but can provide some smoothing through rapid orbital motion with small amplitude. Kim developed software that optimizes dwell as a function of

position and simulates the effects of polishing runs. We installed an orbital polisher and this software on one of the Mirror Lab's 8.4 m polishing machines and used it extensively to figure the GMT mirror with laps between 36 cm and 5 cm diameter, most of them RC laps.[8]

The dwell-control method is very predictable and repeatable. Figure 2 shows a 25 cm RC lap in use and Figure 3 shows the predicted and measured removal for a polishing run with it. Most of the final figuring of the GMT mirror was done using this method. The polishing machine has two spindles, so we kept the stressed lap on one spindle and used it occasionally for large-scale figuring and smoothing of very small-scale structure. (The stressed lap is much stiffer than the RC laps and does more smoothing.) The two methods are complementary. When the stressed lap was used for small-scale smoothing, it generally introduced some unwanted structure on scales of 20-100 cm. We could correct this structure to an acceptable level in a single run of several hours with one of the orbital laps.

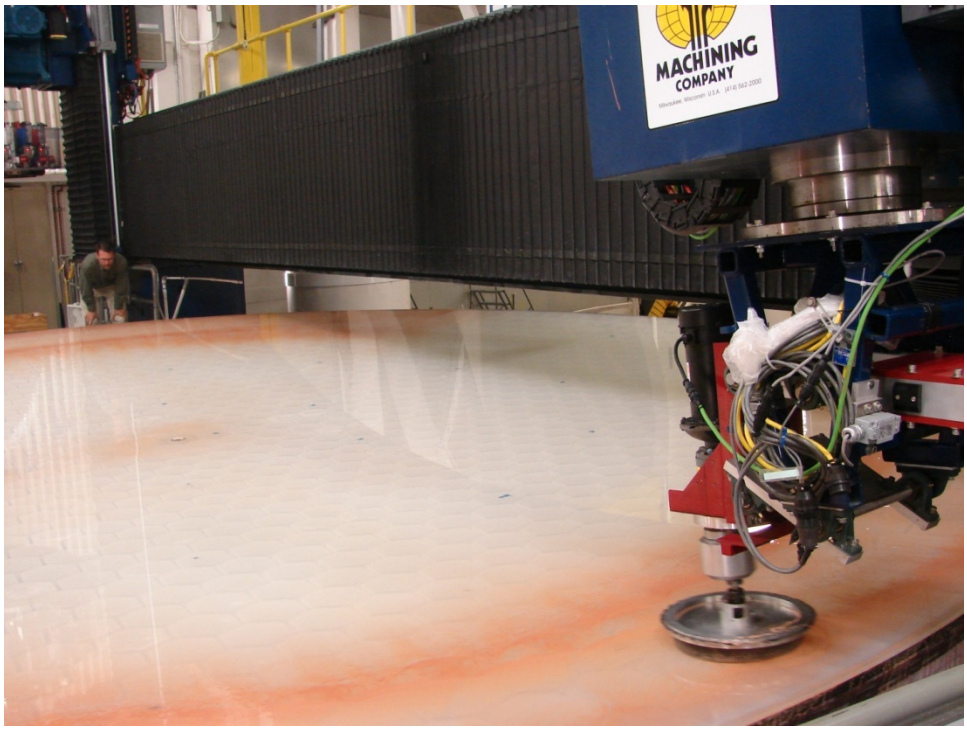

Figure 2. A 25 cm RC lap with an orbital polisher, on the second spindle of the polishing machine, being used for local figuring of the GMT segment.

With the addition of a small-tool figuring capability, we achieved an excellent figure over the inner 8.0 m diameter of the mirror surface within a few months. The last several months of polishing were devoted to the outer 20 cm and especially the outer 10 cm. (The clear aperture is 8.36 m diameter, leaving a 2 cm band with no figure requirement.) Parts of the outer 20 cm had such large slope errors that we could not measure them with the interferometer. This region was eventually brought to an acceptable figure through the use of tools as small as 5 cm and a new measuring system (SCOTS, described in Section 3) with a high dynamic range for slopes. Section 4 presents the results.

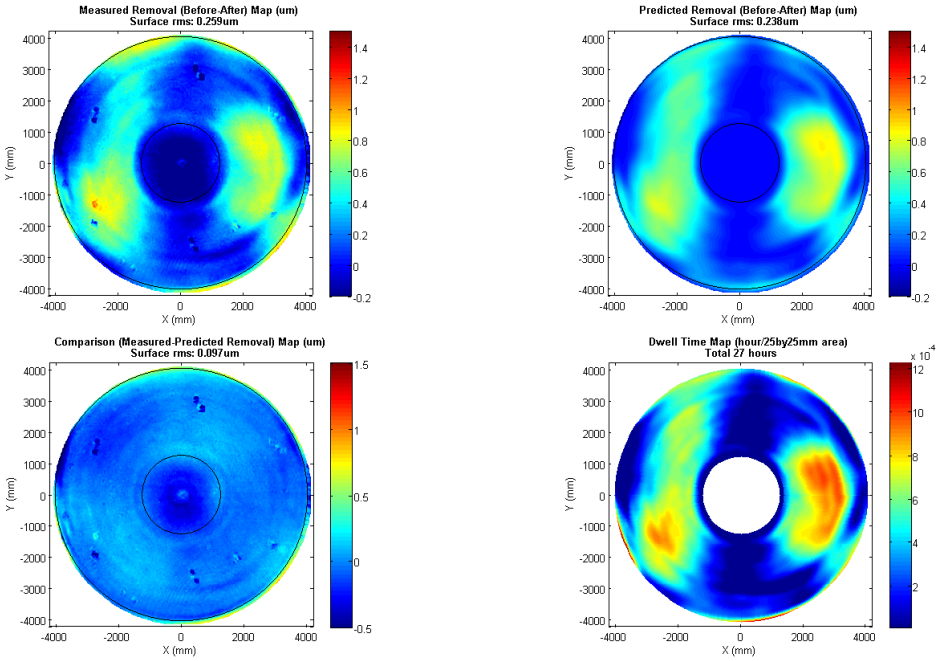

Figure 3. Comparison of predicted removal (top right) and measured removal (top left) for a 27 hour polishing run using a 25 cm RC lap on the GMT segment. Removal is shown as positive, in units of microns. The lower left plot is the difference, measured - predicted removal. The lower right plot is the dwell time as a function of position in arbitrary units. Two black circles in each map represent the boundaries of the tool path. The discrete points in the maps are fiducial markers in the test optics, not real surface features.

3. MEASUREMENTS

3.1 Overview

The GMT measurements are made in a 28 m vibration-isolated test tower that was installed in 2006-07. The tower holds equipment for four optical tests. These tests fulfill a number of high-level requirements: measuring all spatial scales from 2 cm to 8.4 m; measuring low-order aberrations (including focus) to an accuracy that guarantees they can be corrected at the telescope by bending with small forces and residual errors; measuring off-axis distance and clocking angle to an accuracy within allowable motion at the telescope; providing redundancy where a mistake in one test would have serious consequences; and supporting all stages of fabrication from generated to polished surface. The four tests are:

1. A full-aperture interferometric null test, the principal test
2. A full-aperture slope measurement, the Software Configurable Optical Test System (SCOTS)
3. A scanning pentaprism test that measures slopes along any diameter of the segment
4. A scan of the surface with a laser tracker, the Laser Tracker Plus (LT+) system.

Tests 2-4 supplement or verify the principal test in different ways. SCOTS verifies the mid-scale structure and measures small-scale structure that the principal test may not resolve. The pentaprism test verifies the low-order aberrations and segment geometry. LT+ measures radius of curvature to high accuracy and is used to guide loose-abrasive grinding because it does not require a specular surface.

3.2 Principal test

The principal test for GMT is a full-aperture interferometric measurement.[9] It uses a large multi-element null corrector to convert the interferometer's spherical wavefront to the asymmetric template wavefront that matches the ideal segment surface. Figure 4 shows the layout of the test. A 3.75 m spherical mirror (large fold sphere, LFS) at the top of

the test tower folds the beam—making the segment's 36 m radius of curvature fit into the 28 m test tower—and does part of the aspheric compensation. The other two elements of the null corrector are a 76 cm spherical mirror (small fold sphere, SFS) and a 13 cm computer-generated hologram (measurement CGH). These smaller components and the interferometer form the small optical assembly that we call Sam. Sam is mounted in a stiff frame 15 m above the GMT segment.

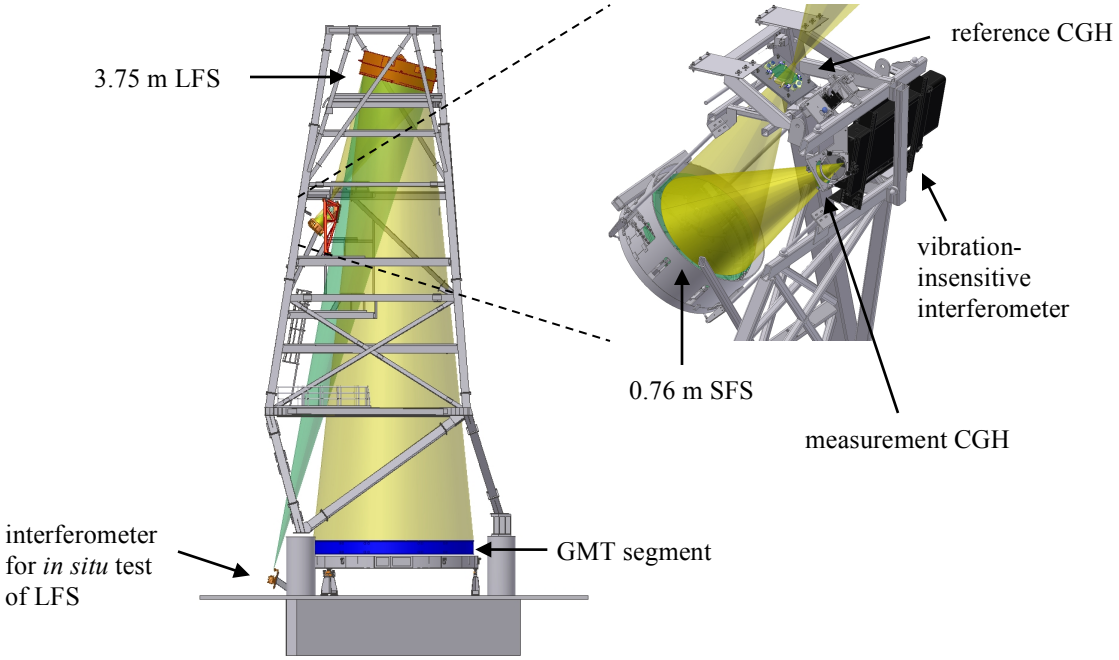

Figure 4. Model of the principal optical test for the GMT off-axis segments, in the 28 m test tower. At right is a blow-up of Sam, comprising the interferometer and first two elements of the null corrector. The reference CGH is inserted for alignment of the test system but removed for the measurement of the GMT segment. Gold light cones represent the measurement of the GMT segment, while the aqua cone in the full model at left represents a simultaneous measurement of the 3.75 m fold sphere.

The interferometer is a high-power vibration-insensitive interferometer from 4D Technology. It has a roughly 25 mW HeNe laser to accommodate the low efficiency of the measurement CGH, and simultaneous phase-shifting to allow accurate measurements over a 65 m round-trip.

Because the null corrector introduces 14 mm of astigmatism and other aberrations, small misalignments cause large wavefront errors. The wavefront is most sensitive to the internal alignment of Sam, which has alignment tolerances around 10 μm. The CGH has a main pattern that does the wavefront correction and a number of other patterns and features that serve as alignment references for the interferometer and SFS. The remaining alignment between Sam, the LFS and the GMT segment is achieved with a laser tracker mounted in the test tower. We align the LFS and GMT not to any component of Sam but to its wavefront. This is done by inserting a reference CGH temporarily at the narrow part of the beam coming from Sam. The reference CGH is designed to return a null wavefront to the interferometer when it is aligned to the outgoing wavefront. The reference CGH, LFS and GMT all have reference targets that can be measured with the laser tracker.

The methods of alignment and expected accuracies are given in References [9] and [10]. For each alignment degree of freedom, we calculated the resulting figure error and simulated the correction using active optics at the telescope, where more accurate wavefront measurements are available. The active correction includes realignment of the segment and bending with the active support, with tight limits on the magnitude of each. The measurement uncertainties for low-order aberrations are large (compared with simple test systems) before active correction, but insignificant after correction. The 2σ uncertainty for astigmatism is 260 nm rms surface, but this can be corrected at the telescope with support forces of only 3 N rms, leaving a residual error of 5 nm rms.

Within Sam, the interferometer and SFS have position adjustments so they can be aligned to the measurement CGH. Sam itself is fixed—once it's aligned, we don't want to move it!—while the reference CGH, LFS and GMT segment are on 6-axis positioners. Alignment of the reference CGH to Sam's wavefront is automated based on the measured wavefront, and alignment of the LFS and GMT segment to the reference CGH is automated based on the laser tracker measurements of all three. The final alignment is a sub-micron tilt adjustment of the GMT segment to eliminate tilt in the interference fringes, and this is accomplished with an actuated adjustment of the volume in the 3 sectors of the hydraulic mirror support.

The LFS is a honeycomb mirror made at the Mirror Lab for this project. Any 3.75 m mirror has figure errors and figure changes large enough to require compensation. A separate vibration-insensitive interferometer from ESDI is mounted at its center of curvature and used to measure its figure at the same time we measure the GMT figure. The LFS figure error is then mapped onto the GMT surface, scaled according to the angle of incidence which varies across the mirror, and subtracted from the measured GMT figure. The mapping requires use of fiducial markers on the LFS, that can be seen in the image in its interferometer as well as the image in the GMT interferometer. We chose to leave these markers permanently on the LFS surface, and they cause 6 small obscurations in the measurements of the GMT surface.

The 3-element null corrector produces an accurate wavefront but a distorted image of the GMT mirror. The magnification is anisotropic and varies by a factor of 2.5 across the aperture. This creates a challenge in determining the locations of high and low zones for figuring the segment, and in determining which parts of the measured surface are in the clear aperture. We find the mapping from the distorted image to the GMT segment by a combination of ray-trace analysis and measurement of fiducial markers.[11] The distortion is described by mapping polynomials that are an optimum set for distortion. High-order distortion between the GMT segment and the measurement CGH is calculated by ray-tracing and requires 37 polynomials. Low-order distortion between the measurement CGH and the interferometer detector is determined by placing 24 fiducial markers at known locations on the GMT segment and measuring their coordinates in the image. (This also determines the magnification, centration and clocking of the image.) The result is a mapping that is accurate to 0.5 cm rms on the GMT surface.

3.3 SCOTS and stitching

The principal test works well over almost all of the 8.4 m aperture, but we had persistent problems measuring the edge because of steep slope errors and limited pixel resolution. The distortion causes the interferometer's pixel spacing to vary from 2-2.5 cm over most of the surface to as much as 5 cm at the edge farthest from the parent vertex. In the early stages of figuring we lost data over large areas near the edge of the mirror. Even in the finished mirror the principal test loses some data in the outer 10 cm in regions with high slope errors and low magnification. We have been able to fill in the missing data using the Software Configurable Optical Test System (SCOTS) developed by Su, Burge and colleagues.[12],[13] This is a full-aperture slope measurement described as a reverse Hartmann test with higher accuracy and resolution than the traditional Hartmann test, and a high dynamic range for slope errors.

The SCOTS measurement is sensitive to alignment of components, which causes uncertainty in low-order polynomials. The SCOTS test of GMT must use the LFS, and there is enough alignment uncertainty that Zernike polynomials through r^5 must be ignored. SCOTS can therefore verify the accuracy of the principal test on scales up to about 4 m but not on larger scales. With those polynomials removed, the two tests agree to 25 nm rms surface. The most valuable information we get from SCOTS, however, is the surface error over the outer 10 cm of the aperture, some of which is missed by the principal test.

We eliminate large-scale uncertainties in SCOTS by stitching the SCOTS map to the interferometric test over a ring $r_1 < r < r_2$ near the edge where both maps have good data. The stitching recipe adjusts the surface and radial slope of the SCOTS map to match the principal test map in the stitching zone, and uses this adjusted SCOTS map to give the surface for $r > r_2$. Rather than adjusting the SCOTS map on a pixel-by-pixel basis, we adjust only spatial frequencies in the azimuth direction that are below some cutoff frequency and leave the high spatial frequencies unchanged. In the stitching zone, the stitched map is a weighted average of the principal test and adjusted SCOTS, with the weighting varying from 100% principal test at r_1 to 100% SCOTS at r_2. For the GMT results presented here, we used r_1= 4.0 m, r_2= 4.1 m, and a cutoff spatial frequency in the azimuth direction of 1 cycle/m.

3.4 Scanning pentaprism and LT+

The pentaprism test measures low-order aberrations to nearly the same accuracy as the principal test.[14]-[17] A mistake in the alignment or implementation of the principal test would cause primarily low-order aberrations, so the pentaprism test is a critical verification. Unlike the interferometric test with its massive null corrector, the pentaprism test uses the telescope's natural geometry to focus a collimated beam onto a detector at the telescope focus. The pentaprism system scans a narrow collimated beam across the segment's diameter and uses the motion of the focused spot to determine the slope errors on the segment surface. Figure 5 shows the test system. Spot motion in the in-scan direction (in the plane containing the pentaprism rail and the telescope's optical axis) is almost immune to changes in the pentaprism's orientation as it scans. Other misalignments, such as a change in tilt of the rail or GMT segment, would cause the spot to move. To compensate for these motions, we use a fixed pentaprism as a reference and measure differential motion between the two spots. The result is measurement of wavefront slope errors in one dimension to an accuracy of about 1 μrad rms.

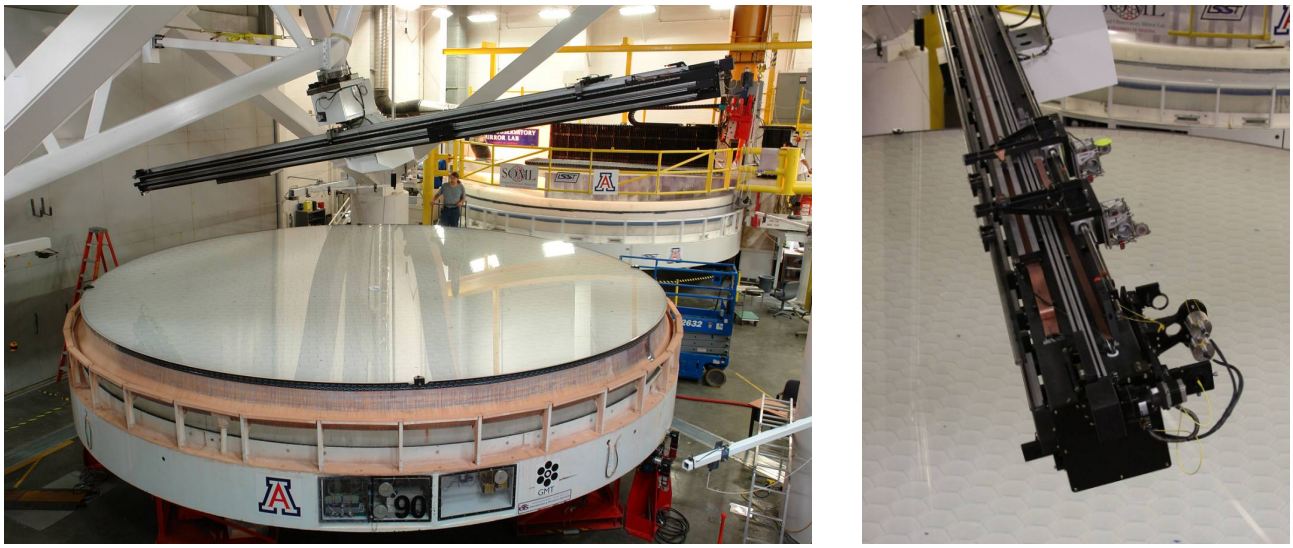

Figure 5. Scanning pentaprism system with GMT segment. Left: the pentaprism rail lies in a plane perpendicular to the telescope's optical axis. Right: A collimator sends light down the rail to (1) a stationary pentaprism-beamsplitter and (2) a scanning pentaprism, both of which deflect the beam parallel to the optical axis. The 2 beams are brought to focus on a detector at the telescope focus.

The rail can rotate to scan any diameter of the segment. We usually scan 5 diameters, giving enough information to accurately determine the Zernike polynomials through r^3 plus spherical aberration. Polynomial fits to the slope measurements yield 2σ uncertainties ranging from 500 nm rms surface for astigmatism to 40 nm rms surface for spherical aberration.

The LT+ system scans the surface with a laser tracker.[14],[18],[19] It is used during generating, loose-abrasive grinding and initial polishing because it does not require a polished surface. The laser tracker (a distance-measuring interferometer, DMI, combined with angular encoders and a pointing servo) is mounted in the test tower 22 m above the GMT segment. We move a standard sphere-mounted retroreflector (SMR) across the surface and measure its position at about 250 points. This motion is automated, with the SMR held in a pneumatic puck with 4 adjustable strings attached. The puck slides on air bearings, lifts the SMR off the glass surface for moves, and sets it down slowly to contact the glass at each sample point.

The tracker's measurement of relative distance is accurate to a fraction of a micron while the angles are accurate to about 1 μrad rms after a special calibration. If the tracker were located at the segment's center of curvature so its line of sight is normal to the segment surface, the surface measurement would be insensitive to errors in the measured angles. Although the test tower does not allow that ideal geometry, the maximum deviation between line of sight and surface normal is 4°, so angular errors couple only weakly into surface errors. This allows a measurement accuracy of about 1

μm rms. Drift of the segment during the scan would increase the errors, so we mount 4 fixed retroreflectors on the edge of the segment, monitor them with fixed DMIs, and compensate for the motion.

The principal test, scanning pentaprism and LT+ all measure the segment's radius of curvature. LT+ is expected to be the most accurate measurement with a 2σ uncertainty of 0.3 mm.

3.5 Compensations

During all measurements, we monitor the 160 support forces and glass temperature at 36 points on the underside of the front facesheet and an equal number on the back plate. We compensate for the resulting figure changes based on finite-element models. The largest compensation is the change in focus (radius of curvature) due to the average difference between front and back of the mirror. A 0.1 K temperature difference causes 1.4 μm rms focus error, equivalent to 0.8 mm in radius of curvature. A ventilation system reduces the temperature difference below 0.02 K in most cases, and the differential measurements are good to about 0.01 K or 0.08 mm in radius. We also compensate for small residual misalignments of the LFS and GMT segment, whose alignment accuracy is limited by the resolution of their stages rather than the tracker measurements. We calculated the sensitivities of different aberrations to misalignments by perturbing the optical design, and verified them experimentally.

4. RESULTS FOR SEGMENT 1

The accuracy requirements for the GMT segments have been described in previous papers.[4],[5] The specification is given as a structure function (mean square wavefront difference between points in the aperture as a function of their separation) that is related to seeing. The GMT specification corresponds to 0.11 arcsecond seeing, with an allowance for an additional 2% loss due to small-scale structure. The 36 m radius of curvature must be controlled accurately because the seven segments must match. Its tolerance is 1.0 mm, corresponding to 1.75 μm rms focus error in the surface, and it must be measured to 0.5 mm. There is a goal of 0.3 mm for both manufacture and measurement. There are also tight tolerances on the segment position in the parent surface. The off-axis distance must be 8710 ± 2 mm with a goal of ±1 mm. The clocking, or rotation about the segment center, must be accurate to 50 arcseconds, equivalent to 1 mm of rotation at the edge.

The figure specification applies to the surface after the simulated active-optics correction described in Section 3.2. Low-order aberrations are very sensitive to segment alignment and can be changed by hundreds of nm with realignments within the tolerances on off-axis distance and clocking. For the simulated correction, repositioning is limited to those tolerances and bending is limited to support forces of 42 N rms over the 160 actuators. (The average actuator force at zenith pointing is 1070 N.) We constrain the forces by using only the first 20 bending modes out of the 157 available modes. For the final test results, the required displacements and bending forces are less than half the allowed amounts.

Figure 6 shows the segment figure after the simulated active correction. The correction applied is a change in off-axis distance by -0.2 mm, clocking by 2 arcseconds, and bending with forces of 16 N rms. The figure shows both the principal test map and the stitched map described in Section 3.3. The principal test map has small areas with missing data or incorrect data in the outer 10 cm. The stitched map is a more accurate representation of the surface. The rms surface error over the 8.36 m clear aperture is 19 nm. Several discrete features in the map, including the bump near r = 3 m, 4:30, are defects in the LFS measurement that is subtracted from the GMT measurement. We have recently worked out a method of removing those defects and will apply it to future data.

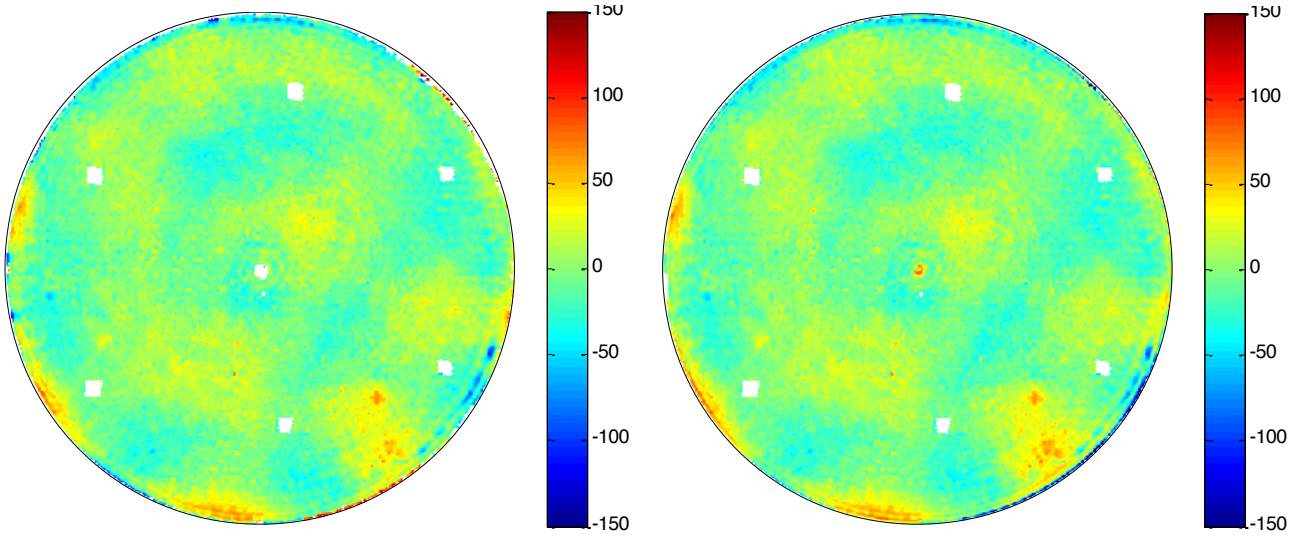

Figure 6. Departure from ideal surface, after simulated active correction, in nm. Left: principal test map (18 nm rms over clear aperture). Right: stitched map with outer 10 cm defined by SCOTS map (19 nm rms over clear aperture). The black circle is the 8.4 m aperture. The center of the parent is to the left.

Figure 7 shows the structure function of the reflected wavefront along with the specification. Data are shown for the 8.36 m clear aperture and a slightly reduced 8.3 m aperture. The data fall within the specification over 8.3 m, but for the 8.36 m aperture the data exceed the specification by less than 10% for separations of 4-7 cm. This is mainly due to the narrow low zone in the lower-right quadrant of the maps in Figure 6, much of which falls inside the 8.36 m aperture. This low zone could be eliminated with further polishing, but it would require removal over a large area using a variety of tool sizes, and the cost outweighs the benefit. The mirror figure and calculated image quality are excellent. Figure 8 shows the point-spread function and encircled energy for the GMT segment alone and for the segment with 0.2 arcsecond seeing. Even in extraordinarily good seeing, the segment adds very little to the image size.

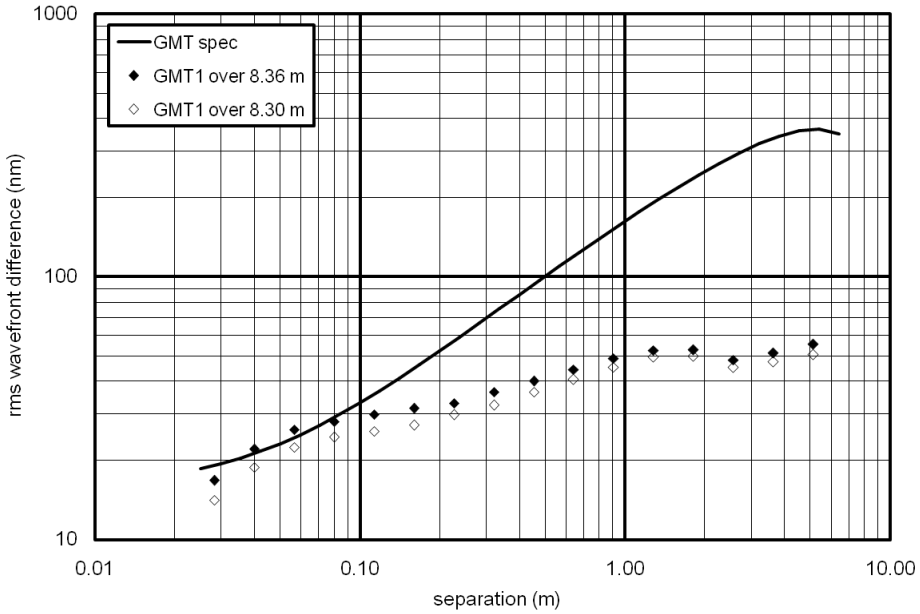

Figure 7. Structure function of the reflected wavefront, plotted as rms wavefront difference as a function of separation. Data are shown for the 8.36 m clear aperture and for a slightly reduced 8.3 m aperture. The solid curve is the specification.

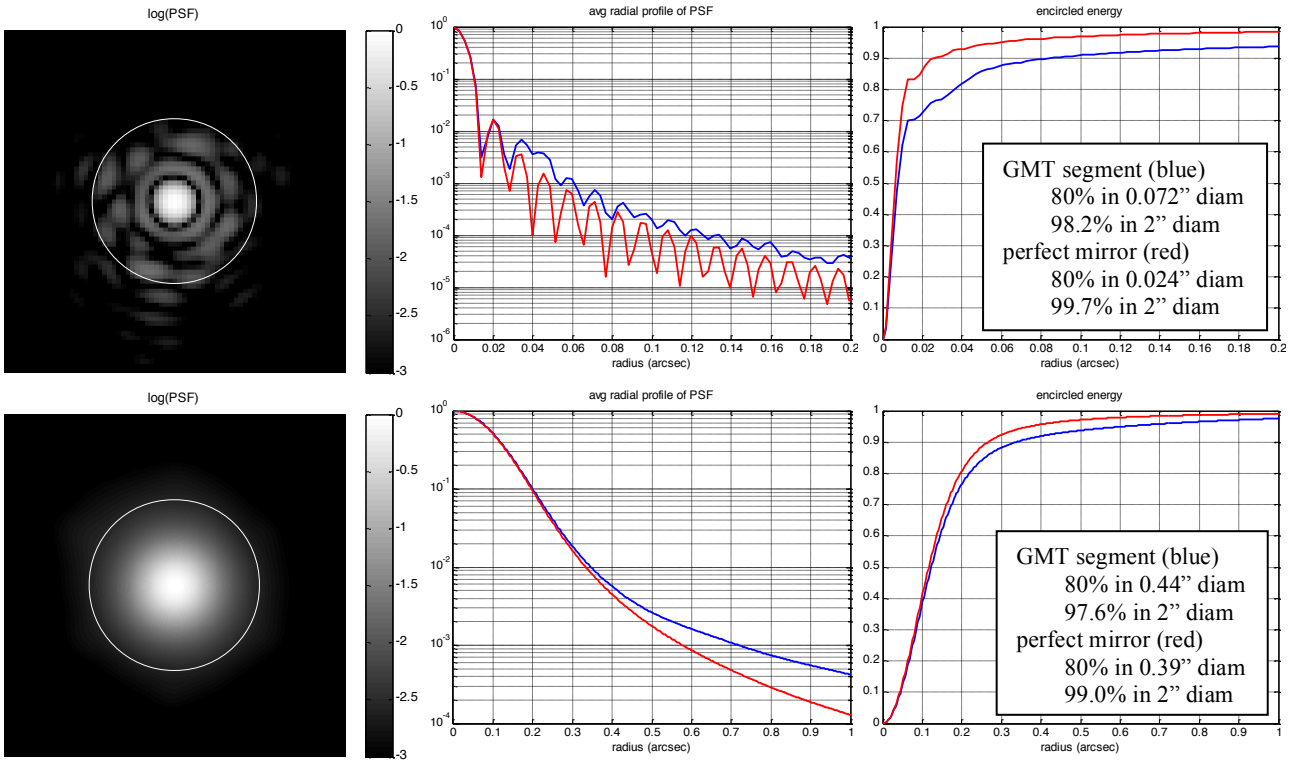

Figure 8. Point-spread function and encircled energy for the GMT segment at λ = 500 nm. Top: segment with no seeing. Bottom: segment in 0.2 arcsecond seeing. The 2D plot and average radial profile of the PSF are on logarithmic scales. The white circle has a diameter of 0.1 arcsecond for no seeing and 1.0 arcsecond for 0.2 arcsecond seeing. The 8.36 m clear aperture is used for the calculations.

On the basis of these results, polishing has ended and we are making a final set of measurements, using all the tests described in Section 3, as part of the acceptance process. The accuracy on small and mid scales has been established by the principal test and SCOTS, so the most important aspect of the acceptance tests is demonstration that the various measurements agree on the segment geometry and low-order aberrations. Previous measurements during fabrication showed good agreement among the tests. We plan is to use the first segment as a measurement standard for at least the next two segments, to guard against any variations due to drift in equipment or modified methods.

The experience gained with the first segment will lead to even better accuracy and much better efficiency for the remaining segments. Manufacture of the first segment was delayed by three issues. The first was development, assembly and debugging of the measurement systems. The tower and all of its components are now complete and only minor improvements are planned for future segments. The second issue causing substantial delays was several discrete mistakes during the early stages of fabrication and measurement. While some mistakes will be made in the future, the ones that delayed the first segment will not happen again due to improved procedures and understanding of the processes. Finally, there were significant delays due to the unexpected difficulties with the stressed lap. We overcame the problems and achieved an excellent figure by using the dwell-control figuring method with smaller RC laps, but this required many months of development and debugging. The dwell-control system is now well established and has demonstrated more efficient figuring than we have had with any previous mirror. We expect to recover more smoothing capability by combining it with a small stressed lap for the remaining segments.

5. SEGMENT 2

With Segment 1 complete, the Mirror Lab can focus on Segment 2 and preparations for the remaining segments. In January 2012, the second segment was spin-cast in conjunction with a gathering of partners and supporters of the GMT. Each spin-casting is a dramatic event. The lightweight honeycomb mirror blank is formed in a matter of hours as

the glass melts and flows into the ceramic fiber mold. This operation gives the mirror its excellent structural and thermal properties: it is several times stiffer, yet lighter, than other large mirrors, and its thermal time constant is reduced to 40 minutes by the thin glass sections and internal ventilation.

The mold, shown in Figure 9, consists of a tub of cast silicon carbide, lined with ceramic fiber on all surfaces and filled with 1681 hexagonal ceramic fiber boxes that will form the voids in the honeycomb mirror. While the spin-casting gives the upper surface of the mirror a symmetric parabolic shape, the mold for a GMT segment is shaped to match the finished segment with its off-axis surface. In this way, the finished facesheet is a uniform 28 mm thick, which optimizes the mechanical and thermal properties. For the off-axis segment no two boxes have the same dimensions. The ceramic fiber boxes are manufactured by Rex Materials and machined to their final shapes at the Mirror Lab before being installed in the mold.

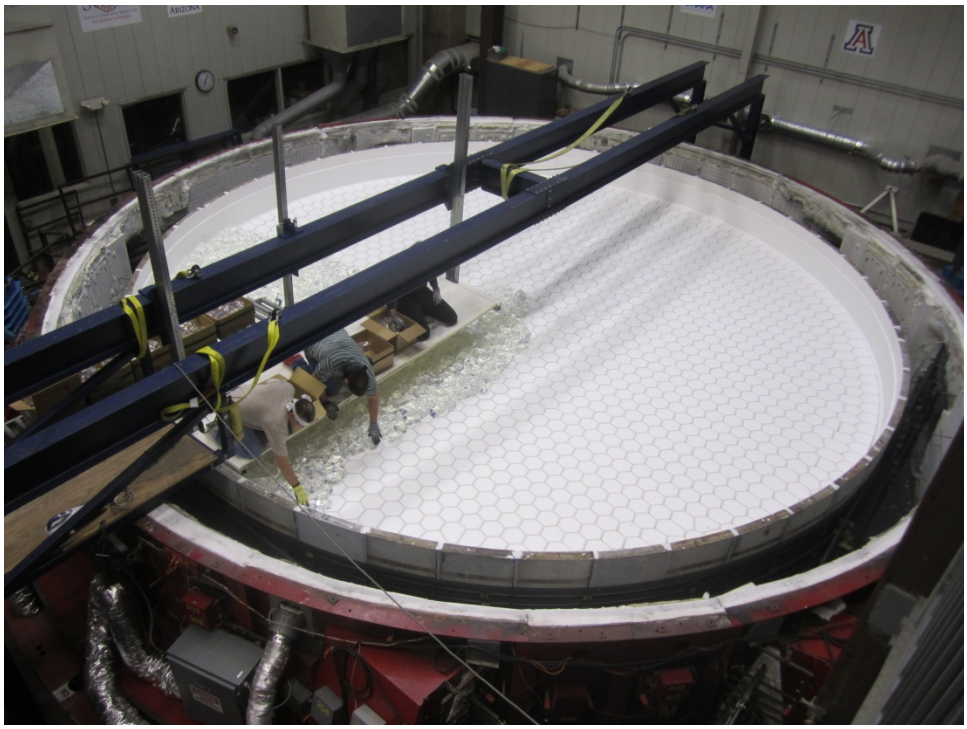

Figure 9. Glass being loaded onto the mold for Segment 2. A temporary bridge supports the workers' platform. The outermost cylinder is the wall of the electric furnace. Inside it is the mold, which is a silicon carbide tub lined with ceramic fiber and filled with 1681 hexagonal boxes of ceramic fiber. The furnace lid is installed after the glass is loaded.

The mold was covered with 18 metric tons of Ohara E6 borosilicate glass in December 2011. Borosilicate is the best candidate material that can be cast in a complex form. The E6 glass is delivered as irregular chunks of about 5 kg with pristine fracture surfaces that melt together without traces of the individual blocks. The quality has always been excellent and continues to improve. The glass for Segment 2 has a coefficient of thermal expansion of 2.8 ppm/K with uniformity of ±0.014 ppm/K over the 58 batches of glass delivered for the casting.

The glass and mold were heated in the electric furnace over a 5-day period. The furnace was rotated at 4.8 rpm starting at 750°C. At the peak temperature of 1165°C the glass has the viscosity of cold honey. It initially formed a fluid layer on top of the ceramic fiber boxes then slowly flowed down the 12 mm gaps between boxes to form the ribs of the honeycomb, and under the boxes to form the 25 mm backplate, while the temperature was held at 1165°C for 4.5 hr. The furnace continued to rotate for 2 days until the mirror had cooled to 650°C, at which point the glass no longer flows under gravity. Figure 10 shows views of the glass before and after melting, taken by cameras mounted in the ceiling of the furnace.

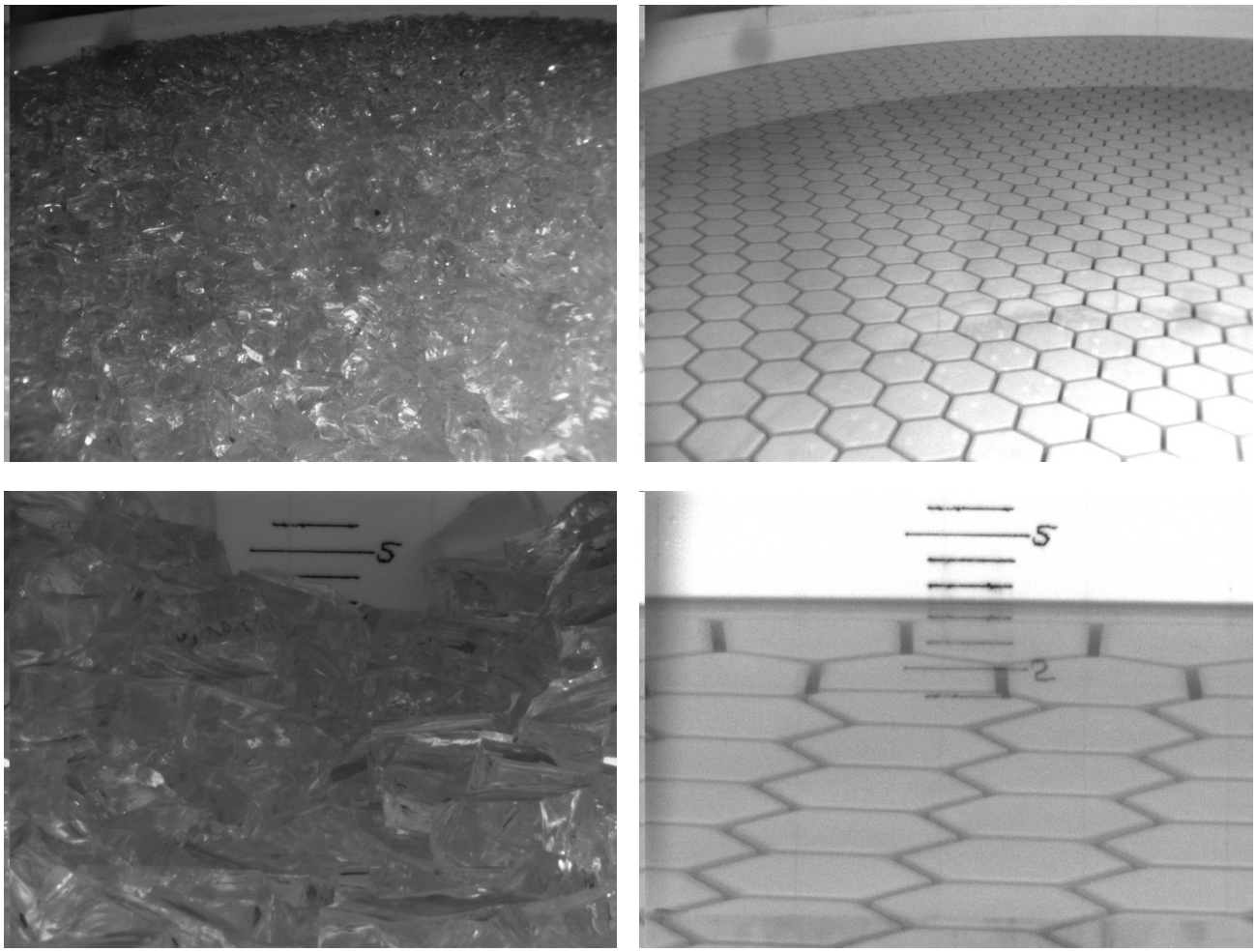

Figure 10. Views of the glass before and after the spin-casting, on January 12 and January 15, 2012, respectively. After the casting, the ceramic fiber boxes are seen through the transparent facesheet. Marks on the wall of the mold indicate height above the boxes in inches. The finished facesheet will be 28 mm (1.1 inch) thick.

The glass still flows microscopically to relieve stress until it cools below 500°C. The stress relaxation time increases from hours to years through the annealing range of about 530°C to 450°C. During this period the mirror was cooled at 0.1 K/hr, reducing the temperature gradient across its thickness to less than 1 K, to minimize the stresses present after it reaches equilibrium at room temperature. It then cooled at a higher rate to room temperature. The casting process took 10 days for heating and casting plus 85 days for annealing and cooling.

After the casting, a handling fixture was bonded to the front surface and the segment was lifted and turned into a vertical plane, giving access to the rear surface. Figure 11 shows the lifting and turning operation. As this paper is written, the trapped ceramic fiber mold pieces are being washed out with high-pressure water hosed through the holes in the back plate. The segment will then be turned face-down and mounted on the 8.4 m grinding machine, where the rear surface and edges are machined and polished. One hundred sixty loadspreaders that form the interface to the mirror support actuators will be surveyed in place and bonded permanently to the rear surface. The segment will then be turned face-up and mounted in the polishing support cell for generating, loose-abrasive grinding and polishing of the front surface.

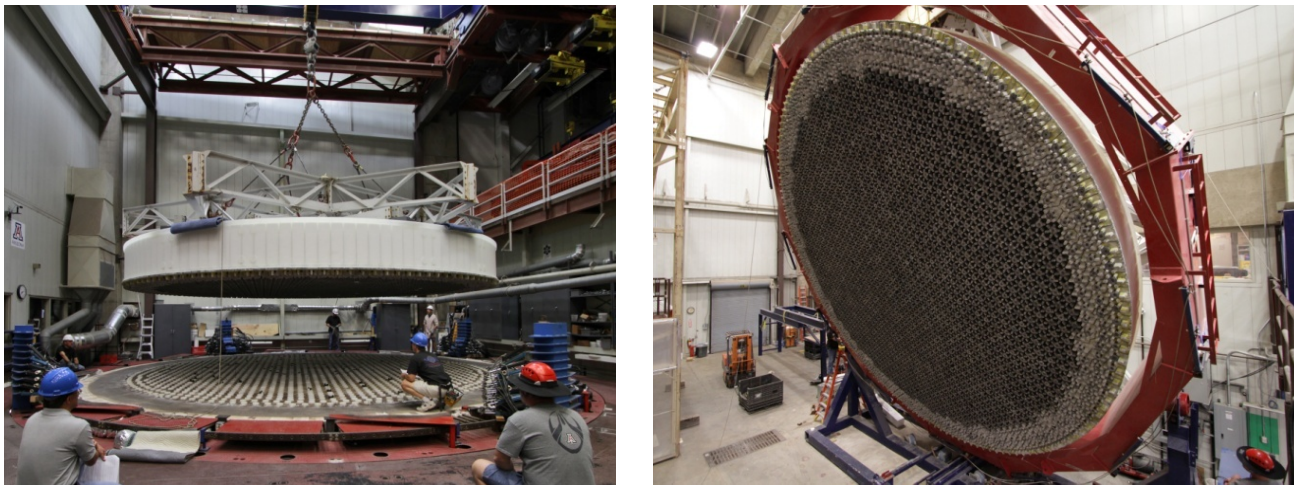

Figure 11. Left: Segment 2 being lifted off the furnace following the casting. Right: the segment in its turning ring, being rotated into a vertical plane for removal of the mold parts. Prior to the lift, the mold was removed from the mirror's side wall where it was accessible, but most of the silicon carbide floor tiles are still attached to the back plate during the lifting operation. Photos by Ray Bertram, Steward Observatory.

6. SEGMENTS 3-8

The Mirror Lab recently began mold construction for Segment 3. Most of the glass (13.5 tons) has been delivered by Ohara and the remaining glass will be in hand by November 2012. Delivery of mold parts will be complete by December 2012. The casting is scheduled for August 2013. Castings will occur at roughly 12 month intervals for the remaining segments, including the spare off-axis Segment 8. It is likely that Segment 4 will be the center segment, giving the GMT Project a close-packed array of 4 segments for testing and commissioning the telescope. We plan to deliver Segments 1-4 to the telescope in 2019, and the remaining segments at 12 month intervals after that. The production cycle is based on simultaneous work on mirrors at each of the 3 stations: casting, generating and grinding, and polishing.

7. CONCLUSION

The first off-axis GMT segment has been finished to an accuracy of 19 nm rms after simulated active correction. The calculated image quality is excellent, with 80% of the light in a 0.074 arcsecond diameter. In exceptionally good 0.2 arcsecond seeing, the mirror would add only 0.05 arcsecond to the diameter containing 80%. During the process of making this mirror, the Mirror Lab built and demonstrated the full suite of tests that will be used for all the GMT segments. The lab overcame figuring difficulties by implementing a new deterministic system that gives more efficient figuring than we had achieved on any previous mirror. A complete system is in place for efficient production of the remaining segments.

Segment 2 was cast in January 2012 and is being prepared for generating. Mold construction and delivery of glass are underway for the casting of Segment 3 in August 2013. The Mirror Lab continues to improve the processes that lead to better quality and more efficient production of the GMT segments.

ACKNOWLEDGEMENTS

This work has been supported by the GMTO Corporation, a non-profit organization operated on behalf of an international consortium of universities and institutions: Astronomy Australia Ltd, the Australian National University, the Carnegie Institution for Science, Harvard University, the Korea Astronomy and Space Science Institute, the Smithsonian Institution, The University of Texas at Austin, Texas A&M University, University of Arizona and University of Chicago.

This material is based in part upon work supported by AURA through the National Science Foundation under Scientific Program Order No. 10 as issued for support of the Giant Segmented Mirror Telescope for the United States Astronomical Community, in accordance with Proposal No. AST-0443999 submitted by AURA.

We thank Nick Woolf for many valuable and enlightening discussions.

REFERENCES

[1] M. Johns, P. J. McCarthy, K. Raybould, A. Bouchez, A. Farahani, J. M. Filgueira, G. H. Jacoby, S. A. Shectman and M. Sheehan, "Giant Magellan Telescope: overview ", *Ground-based and Airborne Telescopes IV*, Proc. SPIE 8444, paper 8444-52 (2012).

[2] S. Shectman and M. Johns, "GMT Overview", *Ground-based and Airborne Telescopes III*, Proc. SPIE 7733, 77331Y (2010).

[3] H. M. Martin, J. R. P. Angel, J. H. Burge, B. Cuerden, W. B. Davison, M. Johns, J. S. Kingsley, L. B. Kot, R. D. Lutz, S. M. Miller, S. A. Shectman, P. A. Strittmatter and C. Zhao, "Design and manufacture of 8.4 m primary mirror segments and supports for the GMT", *Optomechanical Technologies for Astronomy*, Proc. SPIE 6273, 62730E (2006).

[4] H. M. Martin, J. H. Burge, B. Cuerden, W. B. Davison, J. S. Kingsley, W. C. Kittrell, R. D. Lutz, S. M. Miller, C. Zhao and T. Zobrist, "Progress in manufacturing the first 8.4 m off-axis segment for the Giant Magellan Telescope", *Advanced Optical and Mechanical Technologies and Instrumentation*, Proc. SPIE 7018, 70180C (2008).

[5] H. M. Martin, R. G. Allen, J. H. Burge, D. W. Kim, J. S. Kingsley, M. T. Tuell, S. C. West, C. Zhao and T. Zobrist, "Fabrication and testing of the first 8.4 m off-axis segment for the Giant Magellan Telescope", *Modern Technologies in Space- and Ground-based Telescopes and Instrumentation*, Proc. SPIE 7739, 77390A (2010).

[6] D. W. Kim and J. H. Burge, "Rigid conformal polishing tool using non-linear visco-elastic effect", Opt. Express **18**, 2242-2257 (2010).

[7] D. W. Kim, S. Kim and J. H. Burge, "Non-sequential optimization technique for a computer controlled optical surfacing process using multiple tool influence functions", Opt. Express **17**, 21850-21866 (2009).

[8] D. W. Kim, H. M. Martin and J. H. Burge, "Calibration and optimization of computer-controlled optical surfacing for large optics", *Optical Manufacturing and Testing IX*, Proc. SPIE 8126, 812615 (2011).

[9] J. H. Burge, W. Davison, H. M. Martin and C. Zhao, "Development of surface metrology for the Giant Magellan Telescope primary mirror", *Advanced Optical and Mechanical Technologies in Telescopes and Instrumentation*, Proc. SPIE 7018, 701814 (2008).

[10] S. C. West, J. H. Burge, B. Cuerden, W. B. Davison, J. Hagen, H. M. Martin, M. T. Tuell and C. Zhao, "Alignment and use of the optical test for the 8.4m off-axis primary mirrors of the Giant Magellan Telescope", *Modern Technologies in Space- and Ground-based Telescopes and Instrumentation*, Proc. SPIE 7739, 77390N (2010).

[11] P. Zhou, H. M. Martin, C. Zhao and J. H. Burge, "Mapping Distortion Correction for GMT Interferometric Test," *OSA Optical Fabrication and Testing*, paper OW3D.2 (2012).

[12] P. Su, R. E. Parks, L. Wang, R. Angel and J. H. Burge, "Software configurable optical test system: a computerized reverse Hartmann test," *Applied Optics*, Vol 49, Issue 23, pp 4404-4412 (2010).

[13] P. Su, S. Wang, M. Khreishi, Y. Wang, T. Su, R. E. Parks, P. Zhou, M. Rascon, T. Zobrist, H. Martin and J. H. Burge, "SCOTS: A reverse Hartmann test with high dynamic range for Giant Magellan Telescope primary mirror segments", *Modern Technologies in Space- and Ground-based Telescopes and Instrumentation II*, Proc. SPIE 8450, paper 8450-31 (2012).

[14] J. H. Burge, L. B. Kot, H. M. Martin, C. Zhao and T. Zobrist, "Alternate surface measurements for GMT primary mirror segments", *Optomechanical Technologies for Astronomy*, Proc. SPIE 6273, 62732T (2006).

[15] P. Su, J. H. Burge, B. Cuerden and H. M. Martin, "Scanning pentaprism measurements of off-axis aspherics", *Advanced Optical and Mechanical Technologies in Telescopes and Instrumentation*, Proc. SPIE 7018, 70183T (2008).

[16] P. Su, J. H. Burge, B. Cuerden, R. G. Allen and H. M. Martin, "Scanning pentaprism measurements of off-axis aspherics II," *Optical Manufacturing and Testing VIII*, Proc. SPIE 7426, 74260Y (2009).

[17] R. G. Allen, J. H. Burge, P. Su and H. M. Martin, "Scanning pentaprism test for the GMT 8.4 m off-axis segments", *Modern Technologies in Space- and Ground-based Telescopes and Instrumentation*, Proc. SPIE 7739, 773911 (2010).

[18] T. Zobrist, J. H. Burge, W. Davison and H. M. Martin, ”Measurement of large optical surfaces with a laser tracker”, *Advanced Optical and Mechanical Technologies in Telescopes and Instrumentation*, Proc. SPIE 7018, 70183U (2008).
[19] T. L. Zobrist, J. H. Burge and H. M. Martin, “Accuracy of laser tracker measurements of the GMT 8.4 m off-axis mirror segments”, *Modern Technologies in Space- and Ground-based Telescopes and Instrumentation*, Proc. SPIE 7739 (2010).